Acta Radiologica Open
7(1) 1–8

DOI: 10.1177/2058460117751565
journals.sagepub.com/home/arr
SAGE

Effects of diffusion time on non-Gaussian diffusion and intravoxel incoherent motion (IVIM) MRI parameters in breast cancer and hepatocellular carcinoma xenograft models

Mami Iima[1,2], Tomomi Nobashi[1], Hirohiko Imai[3], Sho Koyasu[1,4,5], Tsuneo Saga[1], Yuji Nakamoto[1], Masako Kataoka[1], Akira Yamamoto[1], Tetsuya Matsuda[3] and Kaori Togashi[1]

Abstract

Background: Perfusion-related intravoxel incoherent motion (IVIM) and non-Gaussian diffusion magnetic resonance (MR) parameters are becoming important biomarkers for differentiating malignant from benign tumors without contrast agents. However, diffusion-time dependence has rarely been investigated in tumors.

Purpose: To investigate the relationship between diffusion time and diffusion parameters in breast cancer and hepatocellular carcinoma xenograft mouse models.

Material and Methods: Diffusion-weighted MR images (DWI) were obtained on a 7-T magnetic resonance imaging (MRI) scanner at two different diffusion times (9.6 ms and 27.6 ms) in human breast cancer (MDA-MB-231) and hepatocellular carcinoma (HepG2 and PLC/PRF/5) xenograft mouse models. Perfusion-related IVIM (fIVIM and D*) and non-Gaussian diffusion (ADC_0 and K) parameters were estimated. Parametric maps of diffusion changes with the diffusion times were generated using a synthetic apparent diffusion coefficient (sADC) obtained from $b = 438$ and 2584 s/mm^2.

Results: ADC_0 values significantly decreased when diffusion times were changed from 9.6 ms to 27.6 ms in MDA-MB-231, HepG2, and PLC/PRF/5 groups ($P = 0.0163$, 0.0351, and 0.0170, respectively). K values significantly increased in MDA-MB-231 and HepG2 groups ($P < 0.0003$ and $= 0.0007$, respectively); however, no significant difference was detected in the PLC/PRF/5 group. fIVIM values increased, although not significantly ($P = 0.164$–0.748). The maps of sADC changes showed that diffusion changes with the diffusion time were not homogeneous across tumor tissues.

Conclusion: Diffusion MR parameters in both breast cancer and HCC xenograft models were found to be diffusion time-dependent. Our results show that diffusion time is an important parameter to consider when interpreting DWI data.

Keywords

Non-Gaussian diffusion MRI, intravoxel incoherent motion (IVIM), kurtosis, breast cancer xenograft model, hepatocellular carcinoma (HCC) xenograft model

Date received: 18 July 2017; accepted: 10 December 2017

[1]Department of Diagnostic Imaging and Nuclear Medicine, Kyoto University Graduate School of Medicine, Kyoto, Japan
[2]The Hakubi Center for Advanced Research, Kyoto University, Kyoto, Japan
[3]Division of Systems Informatics, Department of Systems Science, Kyoto University Graduate School of Informatics, Kyoto, Japan
[4]Laboratory of Cancer Cell Biology, Department of Genome Dynamics, Radiation Biology Center, Kyoto University, Kyoto, Japan
[5]Research Center for Advanced Science and Technology, Tokyo University, Tokyo, Japan

Corresponding author:
Mami Iima, Department of Diagnostic Imaging and Nuclear Medicine, Kyoto University Graduate School of Medicine, 54 Shogoin-kawaharacho, Sakyo-ku, Kyoto, Kyoto 606-8507, Japan.
Email: mamiiima@kuhp.kyoto-u.ac.jp

Introduction

Diffusion magnetic resonance imaging (MRI) is undergoing a revival in its application in tumor imaging. Many studies have revealed the potential of diffusion-weighted imaging (DWI) in the detection, diagnosis, and treatment monitoring of various cancers (1,2), including breast cancer (3) and hepatocellular carcinoma (HCC) (4). Recent work has emphasized the importance of non-Gaussian diffusion, which can be investigated using high b values (5,6), as non-Gaussian diffusion is more sensitive to water diffusion hindrance by tissue constitutive elements (cell membranes, fibers, etc.), which might be denser in malignant tissues (7). A higher degree of diffusion hindrance is expected with an increase in diffusion time, as more water molecules have a chance to encounter obstacles. Indeed, the dependency of measured diffusion parameters on diffusion time has been reported in the normal rat brain (8) and in tumors implanted in the mouse brain (9,10). Although diffusion MR-derived parameters were found to be useful for the differentiation of various malignant and benign lesions (5,11,12), to the best of our knowledge, perfusion-related intravoxel incoherent motion (IVIM) and non-Gaussian diffusion MR parameters and their diffusion-time dependence have not been investigated. Their change with different diffusion times may provide important information to characterize tumor tissues and microstructures.

The aim of our study was to investigate the dependency of perfusion-related IVIM parameters (fIVIM and D*) and non-Gaussian diffusion parameters (ADC_0 and kurtosis) MR on the diffusion time in three human cancer xenograft models (based on MDA-MB-231, HepG2, and PLC/PRF/5 cell lines) using a preclinical model at 7-T MRI.

Material and Methods

Animals and tumor implantation

All animal experiments were approved by the Kyoto University Animal Care Committee. One human breast cancer cell line (MDA-MB-231) and two HCC cell lines (HepG2 and PLC/PRF/5), obtained from American Type Culture Collection, Manassas VA, USA, were cultured in Dulbecco's modified Eagle's medium with 10% fetal bovine serum and 1% penicillin streptomycin. MDA-MB-231 cells (4×10^6) were subcutaneously inoculated into the right hind limbs of eight immunodeficient mice (ICR nu/nu 6–8-week-old females; Charles River Laboratories Japan, Yokohama, Japan). HepG2 and PLC/PRF/5 cells (8×10^6) were subcutaneously inoculated into both hind limbs of four and three immunodeficient mice (Balb/c nu/nu 6–8-week-old females; Charles River Laboratories Japan), respectively. Xenografts were allowed to grow for 7–11 weeks to develop tumors of suitable size.

MRI acquisitions

The mice were anesthetized with 1–3% isoflurane in air and maintained still in the magnet using ear bars and a bite bar connected to a nose cone. Respiration and rectal temperature were continuously monitored using an MR-compatible monitoring system (Model 1025, SA Instruments, Inc., Stony Brook NY, USA). The rectal temperature was maintained between 34–37°C.

The mice were imaged on a 7-T MRI scanner (Bruker Biospec, Ettlingen, Germany) using a 1H quadrature transmit/receive volume coil. Effective diffusion time can be approximated as (Δ-δ/3) (ignoring imaging gradient pulses), where δ is the duration of the diffusion gradient pulses and Δ is the interval between the onset of the two diffusion gradient pulses. DWI images were acquired using two different diffusion times: the short diffusion time corresponded to the shortest achievable on our preclinical scanner, while the long diffusion time was chosen to be comparable to what is used on clinical scanners (diffusion gradient duration [δ] 7.2 ms, and diffusion gradient separation [Δ] 12 ms and 30 ms, resulting in effective diffusion times of 9.6 and 27.6 ms, respectively) and 19 b values (0, 5, 10, 20, 30, 50, 70, 100, 200, 400, 600, 800, 1000, 1500, 2000, 2500, 3000, 3500, and 4000 s/mm^2). The two diffusion times and 19 b values were chosen to keep the total acquisition time compatible with a stable anesthetic status for each animal. The SE-EPI acquisition parameters were set as follows: resolution = $250 \times 250\ \mu m^2$; matrix size = 100×100, field of view (FOV) = $25 \times 25\ mm^2$; slice thickness = 1.5 mm; minimum TE compatible with the highest b value to optimize signal-to-noise ratio (SNR) (31.6 ms and 46.9 ms for the short and long diffusion times, respectively); TR = 2500 ms; eight averages; and four segments. The total acquisition time was 50 min 40 s.

T2-weighted (T2W) images were acquired using a Rapid Acquisition with Relaxation Enhancement (RARE) sequence with the following parameters: resolution = $195 \times 195\ \mu m^2$; matrix size = 128×128; FOV = $25 \times 25\ mm^2$; slice thickness = 1.5 mm; effective TE = 56 ms; RARE factor = 8; TR = 2500 ms; and four averages. The total acquisition was 2 min 40 s.

Data analysis

The data analysis was performed on a region-of-interest (ROI) basis using in-house software developed in Matlab (Mathworks, Natick, MA, USA). ROIs in the tumors were drawn manually using the T2W imaging as

a reference to avoid necrotic or hemorrhagic areas. Mean values of perfusion-related IVIM and diffusion parameters were retrieved for each ROI.

Signals acquired for each diffusion time at $b > 500\,s/mm^2$ (free from perfusion-related IVIM effects) were first fitted using the non-Gaussian diffusion kurtosis model[5]:

$$S(b) = [\{S_0 diff \exp[-bADC_0 + (bADC_0)^2 K/6]\}^2 + NCF]^{1/2} \quad (1)$$

where S(b) is raw signal intensity, S_0diff is the theoretical signal that would be obtained at $b = 0\,s/mm^2$ taking only the tissue diffusion component into account, and NCF (noise floor correction factor) is a parameter that characterizes the "intrinsic" Rician noise contribution observed at low signal intensities within amplitude-reconstructed MR images. Noise floor was estimated from the average image background noise across runs (5).

As a second step, the fitted diffusion signal component was subtracted from the measured signal acquired with $b < 500\,s/mm^2$ and the remaining signal was fitted using the perfusion-related IVIM model (5) to get estimates of the flowing blood fraction, fIVIM, and the pseudodiffusion, D*.

$$Sivim(b) = S_0 ivim \exp(-bD^*) \quad (2)$$

and

$$fIVIM = S_0 ivim / (S_0 ivim + S_0 diff) \quad (3)$$

where Sivim is the raw signal intensity after the diffusion component has been removed and S_0ivim is the theoretical signal from perfusion-related IVIM at $b = 0\,s/mm^2$.

A composite, synthetic apparent diffusion coefficient (sADC) was also calculated to generate parametric maps of diffusion changes with the diffusion time as:

$$sADC = \ln[S(Lb)/S(Hb)]/(Hb - Lb) \quad (4)$$

where Lb is a "low key b value" and Hb is a "high key b value" optimized to obtain the highest overall sensitivity to minute changes in both ADC_0 (Gaussian diffusion approximation) and K (non-Gaussian diffusion) induced by changes in tissue microstructure (13). Based on the average ADC_0 and K values obtained in the tissues used in this study, the values for Lb and Hb were set to 438 and $2584\,s/mm^2$, respectively. Maps of sADC changes were computed on a voxel-by-voxel basis as:

$$sADCchange = 100*(sADCshort/sADClong - 1) \quad (5)$$

The diffusion and perfusion-related IVIM parameters with the different diffusion times were compared using a paired *t*-test. *P* values less than 0.05 were considered statistically significant. All the statistical analysis was performed by using statistical software Medcalc (version 11.3.2.0, Mariakierke, Belgium).

Results

The mean and standard deviation of the tumor diameters in the MDA-MB-231 (n = 8), HepG2 (n = 7), and PLC/PRF/5 (n = 6) groups were 12.66 ± 2.90, 10.03 ± 2.02, and 10.87 ± 2.47 mm, respectively. Diffusion and perfusion-related IVIM values depending on the different diffusion times in MDA-MB-231, HepG2, and PLC/PRF/5 tumor xenograft models are provided in Table 1. Box-and-whisker plots of ADC_0 and K values against the diffusion times in the xenograft models of breast cancer and HCC are summarized in Figs 1 and 2.

ADC_0 values significantly decreased in the MDA-MB-231, HepG2, and PLC/PRF/5 groups ($P = 0.0163$, 0.0351, and 0.0170, respectively) when the diffusion time was increased from 9.6 ms to 27.6 ms. The average ADC_0 decrease was similar for all tumor types (−16.5%, −18.5%, and −14.0%, respectively). There was a significant increase in K value ($P = 0.0003$ and 0.0007) with the increased diffusion time in MDA-MB-231 and HepG2 groups. There was no significant difference in K value with different diffusion times in the PLC/PRF/5 group ($P = 0.70$). The average increase in K was very high for both MDA-MB-231 and HepG2 groups (36.0% and 92.4%, respectively), confirming the large increase in diffusion hindrance with the increased diffusion time. There was no significant change in fIVIM and D* values with the increased diffusion time in the MDA-MB-231, HepG2, and PLC/PRF/5 groups.

A plot example of the diffusion-weighted signal decay in the MDA-MB-231 xenograft model is shown in Fig. 3. Representative sADC maps with short and long diffusion times, as well as maps of their sADC change, are shown in Figs 4–6. The patterns of sADC changes with diffusion time were highly heterogeneous in some tumors, revealing tissue features that were not readily visible in the native diffusion-weighted and anatomical images.

Fig. 7 shows the hematoxylin and eosin (H&E) stained images of the three tumor xenograft models. The cellularity appears different among the three models (quantitative data not shown).

Discussion

In this study, perfusion-related IVIM and non-Gaussian diffusion parameters and their variations

Table 1. Diffusion and perfusion-related IVIM values with the two diffusion times in three cancer xenograft models.

	Breast cancer (MDA-MB-231)				HCC (HepG2)			
	9.6 ms	27.6 ms	Change (%)	*P* value	9.6 ms	27.6 ms	Change (%)	*P* value
ADC_0 ($10^{-3}mm^2/s$)	0.74 ± 0.10	0.61 ± 0.07	−16.5 ± 14.3	**0.0163**	0.76 ± 0.15	0.60 ± 0.07	−18.5 ± 16.9	**0.0351**
K	0.62 ± 0.10	0.84 ± 0.15	36.0 ± 16.8	**0.0003**	0.55 ± 0.26	0.91 ± 0.28	92.4 ± 94.0	**0.0007**
fIVIM (%)	7.68 ± 3.99	10.94 ± 10.49	9.6 ± 151.3	0.3328	9.57 ± 8.21	13.48 ± 7.74	−7.9 ± 121.1	0.1640
D* ($10^{-3}mm^2/s$)	6.08 ± 2.03	5.52 ± 098	−2.3 ± 29.6	0.5124	5.00 ± 0.00	6.51 ± 2.90	30.1 ± 58.0	0.2188
	HCC (PLC/PRF/5)							
	9.6 ms	27.6 ms	Change (%)	*P* value				
ADC_0 ($10^{-3}mm^2/s$)	1.05 ± 0.09	0.90 ± 0.11	−14.0 ± 9.7	**0.0170**				
K	0.51 ± 0.09	0.50 ± 0.13	−3.3 ± 16.2	0.7034				
fIVIM (%)	8.31 ± 10.59	9.88 ± 8.75	−144.6 ± 170.9	0.7482				
D* ($10^{-3}mm^2/s$)	11.21 ± 8.23	16.57 ± 18.42	103.7 ± 211.7	0.5569				

Change is the percentage change (%) of parameter values at 9.6 ms and 27.6 ms. *P* values less than 0.05 were considered to indicate statistical significance.

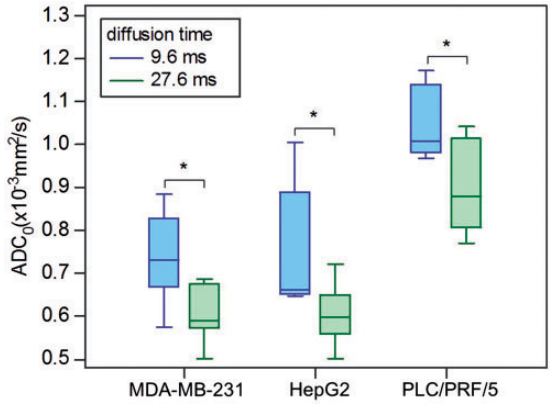

Fig. 1. Box-and-whisker plots of ADC_0 values against the diffusion times in the xenograft models of breast cancer (MDA-MB-231) and HCC (HepG2 and PLC/PRF/5). *$P < 0.05$, comparison of ADC_0 values against diffusion times in each cell line.

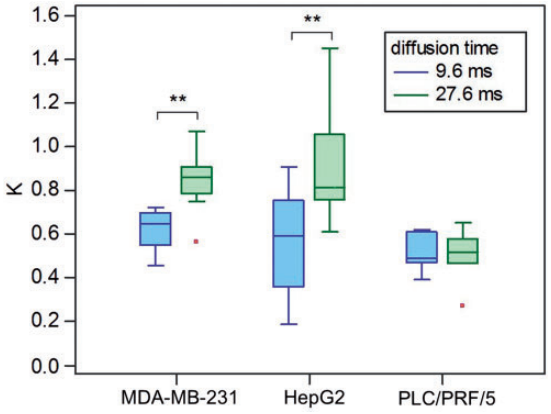

Fig. 2. Box-and-whisker plots of K values against the diffusion times in the xenograft models of breast cancer (MDA-MB-231) and HCC (HepG2 and PLC/PRF/5). **$P < 0.01$, comparison of K values against diffusion times in each cell line.

with short and long diffusion times were acquired in xenograft models of breast cancer and HCC. Such diffusion-time dependence of non-Gaussian diffusion has rarely been evaluated in vivo in xenograft models. A previous study investigated non-Gaussian diffusion signal behavior with diffusion times using a bi-exponential model in a glioma xenograft model, but not in the framework of the diffusion kurtosis model, which is becoming popular (10). Changes in ADC values (Gaussian diffusion approximation) with diffusion times in cellular expression of aquaporin-1 (AQP) have been reported; however, these examinations were performed in vitro and not in a xenograft model (14).

Non-Gaussian diffusion parameters, such as ADC_0 and K, provide information on tissue microstructure. The significant decrease of ADC_0 values and the increase in K values observed in MDA-MB-231 and HepG2 tumors with the higher diffusion time are compatible with the assumption that diffusion hindrance increases with increasing diffusion time, as more water molecules hit many boundaries, such as cell membranes. Such changes could be observed because of the gradient hardware available on preclinical MRI scanners, allowing a broad range of diffusion times to be reached while keeping high b values. With clinical MRI scanners, achievable diffusion times are somewhat longer (30–60 ms) owing to the limitation in gradient hardware (8), although the availability of new, stronger gradient hardware might help in the near future. Long diffusion times may result in the maximization of water exchange effects between tissue compartments that become completely mixed (Gaussian phase). The shorter

diffusion times allowed on preclinical scanners preserve the nature of different water pools in tumors, if they exist, to some extent. Hence, the variation of the diffusion parameters with the diffusion time provides indirect information on tissue function and structure (cell geometry and packing, membrane permeability) (8,15).

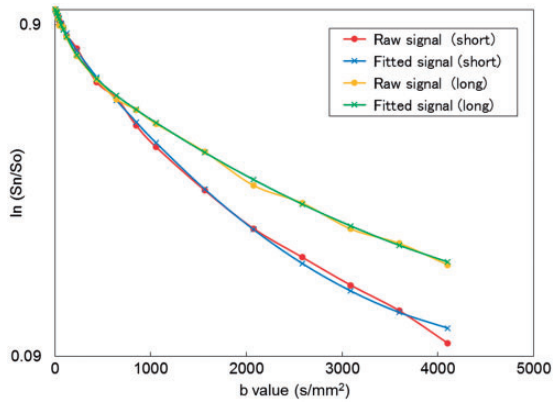

Fig. 3. Comparison of DW signal decay plots in the MDA-MB-231 xenograft model. DW-MRI signal attenuation at two different diffusion times as a function of b values within the MDA-MB-231 xenograft model (their MR images are shown in Fig. 4). Red circle: raw signals with short diffusion time (9.6 ms), blue cross: fitted signals with short diffusion time (9.6 ms), yellow circle: raw signals with long diffusion time (27.6 ms), green cross: fitted signals with long diffusion time (27.6 ms).

Interestingly, the amplitude of ADC_0 changes was similar for all tumor types, although the intrinsic diffusion parameter values (ADC_0 and K) were very different. In the PLC/PRF/5 group, while ADC_0 values decreased when the diffusion time changed from 9.6 ms to 27.6 ms, K remained stable. In contrast, there was a notable shift of K values in the MDA-MB-231 and HepG2 groups. The decrease in ADC_0 value with longer diffusion time observed in our three tumor models is in agreement with the ADC decrease reported in rat brain cortex (8) linked to diffusion hindrance in the neuropile. In tumor tissue, cancer cells (10–15 μm) (16) are much bigger than most of the cellular elements in the brain cortex of rats (<1 μm) (8), while higher cellularity in tumors will lead to more obstacles such as cell membranes, and the hindrance effect observed at high b values is expected to be more prominent, which might result in the change in ADC_0 and K in xenograft models. Interestingly, an ADC increase has been reported in cells expressing human AQP1 water channel (14). Non-Gaussian diffusion imaging using different diffusion times might have the potential to evaluate AQP receptor density and activity in tumors known to overexpress AQP receptors.

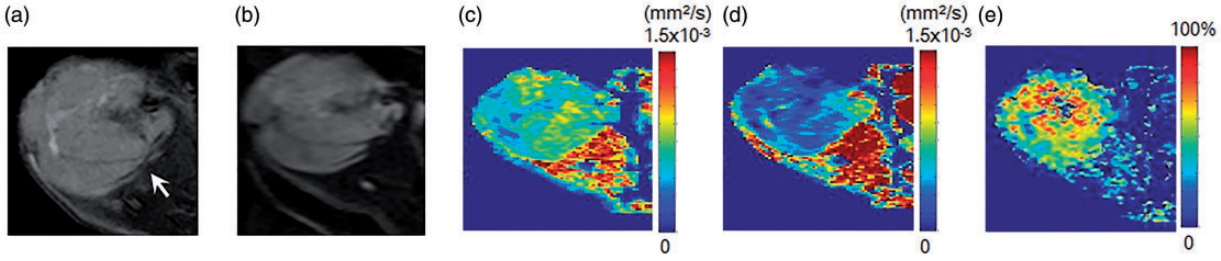

Fig. 4. MR images of an implanted breast cancer (MDA-MB-231) xenograft model. (a) T2W image, (b) DWI, (c, d) sADC maps with short diffusion time (9.6 ms) and long diffusion time (27.6 ms), and (e) sADC change map. Arrow on T2W image indicates the tumor (13.4 mm in diameter). The tumor shows relatively high (yellow-green) sADC at the short diffusion time and low (blue) sADC at the long diffusion time. In contrast, muscle shows high (red-yellow) sADC at both diffusion times. The sADC change in the tumor is striking, while there is very little sADC change in the muscle.

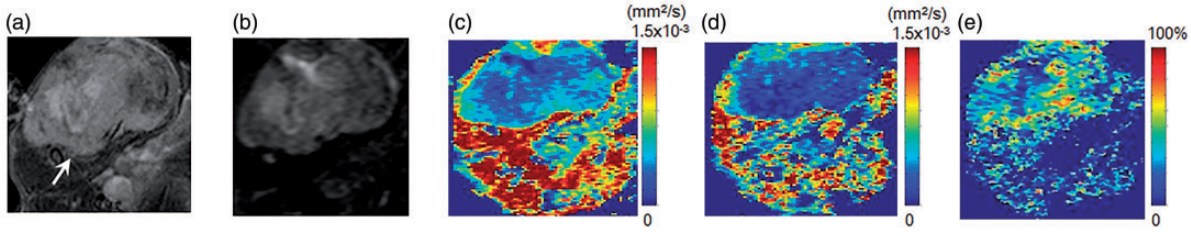

Fig. 5. MR images of a breast cancer (MDA-MB-231) xenograft model. (a) T2W imaging, (b) DWI, (c, d) sADC maps with short diffusion time (9.6 ms) and long diffusion time (27.6 ms), and (e) sADC change map. Arrow on T2W imaging indicates the tumor (16.0 mm in diameter). sADC change in the central part of the tumor can be appreciated only on the sADC change map.

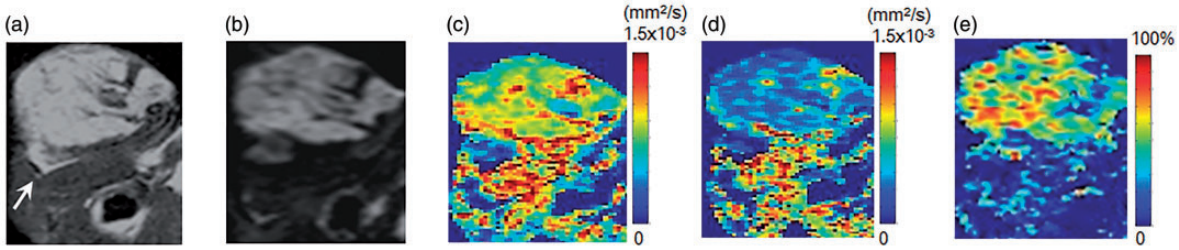

Fig. 6. MR images of a HCC (PLC/PRF/5) xenograft model. (a) T2W imaging, (b) DWI, (c, d) sADC maps with short diffusion time (9.6 ms) and long diffusion time (27.6 ms), and (e) sADC change map. Arrow on T2W imaging indicates the tumor (11.0 mm in diameter). The tumor is homogenous, and sADC clearly decreased with the longer diffusion time.

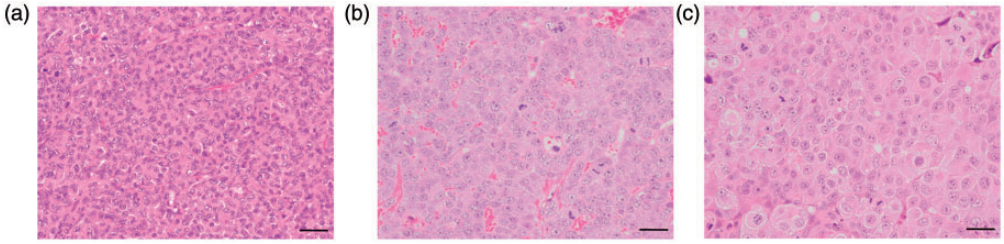

Fig. 7. H&E images of three tumor xenograft models in the study. (a) MDA-MB-231, (b) HepG2, and (c) PLC/PRF/5 tumor xenograft models (magnification 400×, scale-bar = 20 μm).

The observed kurtosis behavior with diffusion time may thus reflect differences in the tumor tissue microstructures. Indeed, differences in the expression levels of extracellular matrix and E-cadherin between HepG2 and PLC/PRF/5 cells have been reported (17). The change of K value with diffusion time has been reported as biphasic in the rat brain by Pyatigorskaya et al. (8). The authors found the first increase in K value from 0.35 to 0.61 at very short diffusion times (1.9–9.2 ms), as diffusion hindrance increased. Then, K value decreased from 0.61 to 0.51 at relatively longer diffusion times (9.2–29.2 ms) when diffusion of water becomes homogeneous throughout the tissue (Gaussian approximation). Hence, the absence of changes in K observed in PLC/PRF/5 tumor xenografts suggests that water diffusion was probably in the Gaussian approximation range at the diffusion times used in this study. This finding points out to a limitation of this study, namely the use of only two diffusion times. This limitation resulted from the requirement to keep the total acquisition time compatible with a stable anesthetic status for each animal, considering that 19 b value signals were acquired.

A mild increase in fIVIM was noted, although the difference was not significant, as in another study investigating IVIM in measuring cerebral perfusion (18). No significant difference of D* was found among any tumor groups.

Maps of sADC changes were useful to highlight features in the tissues that were clearly heterogeneous, a new method of tumor characterization. Such maps combine effects of both Gaussian (ADC_0) and non-Gaussian (K) diffusion. For instance, the area with the largest sADC change corresponds to the area with low sADC value at the longer diffusion time in tumor, suggesting the most proliferating or active part of the tumor (Figs. 4 and 6). However, no sADC change was observed in the center of some tumors, although sADC was low, and there were no findings of necrosis on T2W imaging or DW images in Fig. 5 or in the H&E image in Fig. 7. This pattern might reflect some evolution in the cells' aggressiveness. Further investigation, including histopathological correlation as well as the in vivo association between diffusion times and membrane water channels, such as aquaporins, is needed. Individual sADC values, however, were found noisy and were not reported, as the sADC is calculated using only two b values, while ADC_0 and K were estimated taking into account all 19 b value acquisitions.

Although previous literature suggests no significant difference of mean diffusivity (MD) values with TE, both at 1.5-T and 3-T in white matter of rhesus monkeys (19), one limitation of our study is that two different TEs were used, depending on the diffusion time, to minimize the TE value for each sequence to optimize SNR; hence, the DW signal acquired at each diffusion time had a different degree of T2 weighting. In principle, T2 effects are removed when calculating diffusion intrinsic parameters (ADC_0 and K), with the model used for this study. However, the Kurtosis model is

only an approximation and TE dependence might exist, as the tissue components present in each image voxel likely have different T2s. However, as shown in the supplementary figure, variations of the diffusion parameters with the diffusion times were much larger than with TEs, indicating that the diffusion time is the most significant factor affecting the diffusion parameters.

Furthermore, the flowing blood fraction of the perfusion-related IVIM model (fIVIM) is T2W, as the blood and tissue have different T2 values. However, no significant difference in fIVIM values were found with the two diffusion times, although different TE values were used. Last, variable tumor tissue components with different diffusion coefficients could also have some influence on the changes in diffusion and IVIM parameters (20).

Our results also underline the sensitivity of estimated diffusion parameters to diffusion time owing to the hindrance effect observed at high b values, and demonstrate the effect of the diffusion time on quantitative diffusion measurements. This is an important point to consider for the reproducible application of quantitative diffusion MRI, as the diffusion time is not commonly reported in routine clinical MRI. Breast tissues have been proven to be time-dependent at very long diffusion times as well (21). Hence, there is a need to routinely provide diffusion times and TEs when reporting and interpreting diffusion parameter values, both in preclinical and clinical settings. This is especially true in multi-center studies, as diffusion times may vary across protocols, sites, or MRI vendors, even when using the same set of b values. Non-Gaussian diffusion MR parameters were diffusion time-dependent in the breast cancer and HCC xenograft models. A heterogeneous sADC change was noted in tumors using two different diffusion times. The interpretation of ADC_0 and K value needs caution when acquired with different diffusion times. Clearly, further work is necessary to validate our findings with a larger sample to increase statistical significance, as well as with other tumor models.

In conclusion, diffusion MR parameters in breast cancer and HCC xenograft models showed diffusion time-dependence. This time dependence might provide insight on water compartmentalization and exchange in tissues, a potential source of characterization. Our results emphasize the importance of reporting diffusion times with DWI data.

Acknowledgements

The authors thank Ms. Tomiko Ito for her support with the mice used in this study. They also thank Dr. Libby Cone from Edanz Group Japan for editing a draft of this manuscript. The pathological images were obtained at the Center for Anatomical, Pathological and Forensic Medical Researches, Graduate School of Medicine, Kyoto University.

Declaration of conflicting interests

The author(s) declared no potential conflicts of interest with respect to the research, authorship, and/or publication of this article.

Funding

The author(s) received the following financial support for the research, authorship, and/or publication of this article: Hakubi Project and JSPS Grant-in-Aid for Young Scientists (B) (15K19786).

Supplementary Material

Supplementary material is available for this article online.

References

1. Padhani AR, Koh D-M, Collins DJ. Whole-body diffusion-weighted MR imaging in cancer: current status and research directions. Radiology 2011;261:700–718.
2. Padhani AR, Liu G, Mu-Koh D, et al. Diffusion-weighted magnetic resonance imaging as a cancer biomarker: consensus and recommendations. Neoplasia 2009;11:102–125.
3. Partridge SC, Nissan N, Rahbar H, et al. Diffusion-weighted breast MRI: Clinical applications and emerging techniques. J Magn Reson Imaging 2017;45:337–355.
4. Gluskin JS, Chegai F, Monti S, et al. Hepatocellular carcinoma and diffusion-weighted MRI: detection and evaluation of treatment response. J Cancer 2016;7: 1565–1570.
5. Iima M, Yano K, Kataoka M, et al. Quantitative non-Gaussian diffusion and intravoxel incoherent motion magnetic resonance imaging: differentiation of malignant and benign breast lesions. Invest Radiol 2015;50:205–211.
6. Iima M, Reynaud O, Tsurugizawa T, et al. Characterization of glioma microcirculation and tissue features using intravoxel incoherent motion magnetic resonance imaging in a rat brain model. Invest Radiol 2014; 49:485–490.
7. Yuan J, Yeung DKW, Mok GSP, et al. Non-Gaussian analysis of diffusion weighted imaging in head and neck at 3T: a pilot study in patients with nasopharyngeal carcinoma. PLOS ONE 2014;9:e87024.
8. Pyatigorskaya N, Le Bihan D, Reynaud O, et al. Relationship between the diffusion time and the diffusion MRI signal observed at 17.2 Tesla in the healthy rat brain cortex. Magn Reson Med 2014;72:492–500.
9. Reynaud O, Winters KV, Hoang DM, et al. Surface-to-volume ratio mapping of tumor microstructure using oscillating gradient diffusion weighted imaging. Magn Reson Med 2016;76:237–247.
10. Hope TR, White NS, Kuperman J, et al. Demonstration of Non-gaussian restricted diffusion in tumor cells using diffusion time-dependent diffusion-weighted magnetic resonance imaging contrast. Front Oncol 2016;6:179.
11. Winfield JM, Orton MR, Collins DJ, et al. Separation of type and grade in cervical tumours using non-mono-exponential models of diffusion-weighted MRI. Eur Radiol 2017;27:627–636.

12. Lu Y, Jansen JF, Mazaheri Y, et al. Extension of the intravoxel incoherent motion model to non-gaussian diffusion in head and neck cancer. J Magn Reson Imaging 2012;36:1088–1096.
13. Iima M, Le Bihan D. Clinical intravoxel incoherent motion and diffusion MR imaging: past, present, and future. Radiology 2016;278:13–32.
14. Mukherjee A, Wu D, Davis HC, et al. Non-invasive imaging using reporter genes altering cellular water permeability. Nat Commun 2016;7:13891.
15. Niendorf T, Norris DG, Leibfritz D. Detection of apparent restricted diffusion in healthy rat brain at short diffusion times. Magn Reson Med 1994;32:672–677.
16. Park S, Ang RR, Duffy SP, et al. Morphological differences between circulating tumor cells from prostate cancer patients and cultured prostate cancer cells. PLoS ONE 2014;9:e85264.
17. Lin RZ, Chou LF, Chien CC, et al. Dynamic analysis of hepatoma spheroid formation: roles of E-cadherin and beta1-integrin. Cell Tissue Res 2006;324:411–422.
18. Fournet G, Li J-R, Cerjanic AM, et al. A two-pool model to describe the IVIM cerebral perfusion. J Cereb Blood Flow Metab 2017;37:2987–3000.
19. Qin W, Yu CS, Zhang F, et al. Effects of echo time on diffusion quantification of brain white matter at 1.5T and 3.0T. Magn Reson Med 2009; 61: 755–760.
20. Le Bihan D, Poupon C, Amadon A, et al. Artifacts and pitfalls in diffusion MRI. J Magn Reson Imaging 2006; 24:478–488.
21. Teruel JR, Cho GY, Moccaldi R, et al. Stimulated echo diffusion tensor imaging (STEAM-DTI) with varying diffusion times as a probe of breast tissue. J Magn Reson Imaging 2017;45:84–93.